

Resonant ion-dip infrared spectroscopy of the S_4 and D_{2d} water octamers in benzene-(water) $_8$ and benzene $_2$ -(water) $_8$

Christopher J. Gruenloh, Joel R. Carney, Fredrick C. Hagemeister, Caleb A. Arrington,^{a)} and Timothy S. Zwier^{b)}

Department of Chemistry, Purdue University, West Lafayette, Indiana 47907-1393

Sharon Y. Fredericks,^{c)} John T. Wood III, and Kenneth D. Jordan^{b)}

Department of Chemistry, University of Pittsburgh, Pittsburgh, Pennsylvania 15260

(Received 20 April 1998; accepted 20 July 1998)

The techniques of resonant two-photon ionization (R2PI), UV–UV (ultraviolet) hole-burning, and resonant ion-dip infrared (RIDIR) spectroscopies have been employed along with density functional theory (DFT) calculations to assign and characterize the hydrogen-bonding topologies of two isomers each of the benzene-(water) $_8$ and (benzene) $_2$ (water) $_8$ gas-phase clusters. The BW_8 isomers (B =benzene, W =water) have R2PI spectra which are nearly identical to one another, but shifted by about 5 cm^{-1} from one another. This difference is sufficient to enable interference-free RIDIR spectra to be recorded. As with smaller BW_n clusters, the BW_8 clusters fragment following photoionization by loss of either one or two water molecules. The OH stretch IR spectra of the two BW_8 isomers bear a close resemblance to one another, but differ most noticeably in the double-donor OH stretch transitions near 3550 cm^{-1} . Comparison to DFT calculated minimum energy structures, vibrational frequencies, and infrared intensities leads to an assignment of the H-bonding topology of the BW_8 isomers as nominally cubic water octamers of S_4 and D_{2d} symmetry surface attached to benzene through a π H-bond. A series of arguments based on the R2PI and hole-burning spectra leads to an assignment of additional features in the R2PI spectra to two isomers of B_2W_8 . The OH stretch RIDIR spectra of these isomers show them to be the corresponding S_4 and D_{2d} analogs of B_2W_8 in which the benzene molecules each form a π H-bond with a different dangling OH group on the W_8 sub-cluster. © 1998 American Institute of Physics. [S0021-9606(98)00140-8]

I. INTRODUCTION

Many of the unusual properties of water arise out of its special ability to form networks of hydrogen bonds in which individual molecules act simultaneously as both hydrogen bond donor and acceptor. In ice, this hydrogen-bonding versatility produces an unusual number of structurally distinct phases which form with changing temperature and pressure.¹ The hydrogen-bond coordination number in all such phases is four, with each water molecule donating its two hydrogens to hydrogen bonds (H-bonds hereafter) and accepting two others from its neighbors. Even in liquid water, the average coordination number is near four.² However, at the surfaces of liquid water, ice, and aerosols, in aqueous solutions containing nonpolar solutes, and in other restricted or water-deficient environments, water molecules with unoccupied H-bonding sites will be prevalent. The preferred structures, the degree of cooperative strengthening, and the magnitude of the dynamic coupling in such H-bond-deficient networks are

largely unexplored. Yet, it is precisely in such environments that water takes on unusual properties both as solvent and as reaction partner.

Recently, spectroscopic studies of gas-phase water clusters have provided new insight to the structures, energetics, and dynamics of networks of H-bonds.³ In this regard, the study of water clusters above the pentamer is particularly important because it is for these larger clusters that three-dimensional structures are energetically favored over simple cyclic structures.^{4,5}

The water octamer presents a new H-bonding structural motif that is calculated to be strongly favored over all others; namely, a H-bonded cube. The water octamer was first studied by Stillinger and David⁶ using a polarization model. These authors reported a hexagonal icelike structure, containing nine nearly linear H-bonds. Since then, however, both *ab initio*^{7–13} and model-potential^{13–19} calculations have predicted that the lowest energy structure of the W_8 cluster is nominally cubic with the oxygen atoms of the water molecules taking up positions at the corners of the cube. There are 14 cubic W_8 isomers, each containing 12 H-bonds that differ primarily in the orientations of the H-bonds.^{20,21} As shown in Fig. 1, two of these cubic structures, with S_4 and D_{2d} symmetry, are calculated to be about 2 kcal/mol more strongly bound than the next nearest cubic isomer.¹³ The S_4 and D_{2d} structures may be viewed as a fusion of two cyclic

^{a)}Present address: Dept. of Chemistry, Central Washington University, Ellensburg, WA 98926.

^{b)}Authors to whom correspondence should be addressed. Electronic mail: zwier@chem.purdue.edu; jordan@psc.edu

^{c)}Present address: Dept. of Chemistry, Bloomsburg University, Bloomsburg, PA 17815.

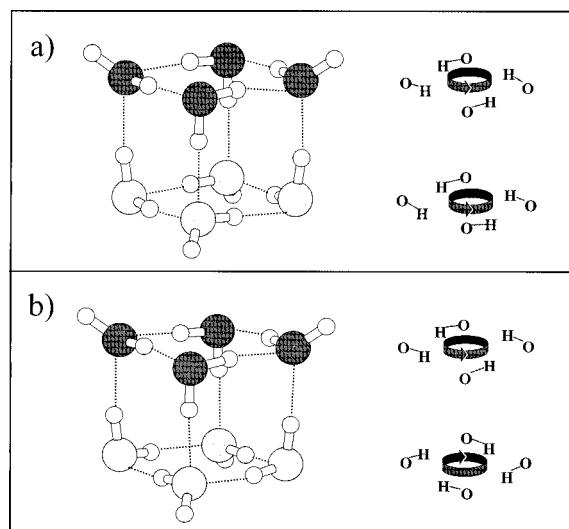


FIG. 1. The S_4 (a) and D_{2d} (b) water octamers, viewed as composites of two cyclic tetramers. The S_4 and D_{2d} W_8 species differ primarily in the orientation of hydrogen bonds within the cubes. Hydrogen-bond donation in the two tetramer cycles occurs with the “same sense” in the S_4 structure and the “opposite sense” in the D_{2d} structure.

tetramers which are bound together by four of the eight “dangling” O–H groups on the cyclic tetramers. The eight water molecules which occupy the corners of the cube are all tri-coordinated, four as double acceptor–single-donor (AAD) and four as single-acceptor–double-donor (ADD) sites. The S_4 and D_{2d} isomers differ primarily in the direction of H-bond donation in the tetramer sub-units, with donation occurring in the same direction in the S_4 species [Fig. 1(a)] and in the opposite direction in the D_{2d} species [Fig. 1(b)].^{12,13}

Beyond the intrinsic beauty of these cubic structures, their study has several motivations. First, the fact that all water molecules in cubic W_8 are tri-coordinated raises the prospect of studying tri-coordinated water molecules free from the tetrahedrally coordinated ones that dominate bulk water and ice. Previous studies have identified these tri-coordinated molecules at the surface of ice^{22–26} using Fourier-transform infrared (FT-IR) spectroscopy and at the vapor–water interface²⁷ from vibrational sum-frequency generation spectroscopy. Second, the cubic water octamers have been proposed as “building blocks” for larger cubic and cuboid structures^{13,28,29} which are among the lowest-energy structures for W_{12} , W_{16} , and W_{20} . Third, the study of gas-phase clusters of benzene and water can provide benchmarks against which the accuracy of current and future H_2O – H_2O and C_6H_6 – H_2O intermolecular potentials can be tested.^{13,30–33} Much work is currently focusing on the importance of many-body terms in these potentials and their effects in cooperatively strengthening the H-bonds in H-bonded networks. Determination of accurate many-body potentials for these systems is essential for better understanding of the molecular-scale interactions that are manifested in many condensed phase properties of water and its solutions with other molecules, including proteins.

The experimental study of small water clusters^{3,5,34–44} is complicated by (i) the range of cluster sizes produced in supersonic expansions, (ii) cluster fragmentation following

ionization in mass-selected studies, and (iii) the increasing number of isomers which can be formed as the cluster size increases. Several clever routes to overcome these difficulties have been put forward, including careful isotopic concentration studies,^{3,5,40–43} scattering methods,^{44–46} and mass-selected double-resonance methods.^{4,47–61}

Our group has addressed the issues of neutral cluster size selection by forming benzene_{*m*}–(H_2O)_{*n*} clusters (denoted B_mW_n) and recording their size- and conformation-selected IR spectra in the OH stretch fundamental region using the technique of resonant ion-dip infrared spectroscopy (RIDIRS).^{4,12,47,58–61} By incorporating a benzene molecule into the cluster as a weakly interacting, surface-attached probe molecule, individual vibronic transitions of a given size and conformation can be interrogated with both mass and wavelength selectivity using resonant two-photon ionization (R2PI) time-of-flight mass spectroscopy (TOFMS).^{62,63} Furthermore, hole-burning spectroscopies^{12,59} have been employed to divide complex R2PI spectra into component parts arising from different species present in the same mass channel. The infrared spectra of each of these species can then be recorded free from interference from one another using RIDIR spectroscopy.

The RIDIRS technique provides substantial insight to the H-bonding topology of the clusters. Because the OH bond vibrates directly against the H-bond, the vibrational frequencies and infrared intensities of the OH stretch fundamentals are sensitive functions of the number, type, and strength of H-bonds in which each OH group participates. In liquid water and ice, where OH groups experience a wide range of different H-bonding environments, the OH stretch infrared absorption is spread over more than 700 cm^{-1} , extending from 3000 to 3700 cm^{-1} .^{1,64} By studying expansion-cooled, gas-phase BW_n clusters of known composition, it is possible to resolve the individual OH stretch transitions of a single H-bonding configuration, determine their spectral signatures, and probe the magnitude and strength of the coupling between OH groups in the network. Recent studies from our group have employed RIDIR spectroscopy to record such size-selected IR spectra of smaller BW_n clusters.^{4,12,47,58} In all cluster sizes studied, the water molecules were bound together in a single aggregate and attached to benzene by a π H-bond between a dangling OH on the W_n sub-cluster and the π cloud of benzene.

In this paper, we present the UV and IR spectral signatures of two isomers of the water octamer complexed to either one or two benzene molecules. A brief report of the BW_8 results has been published elsewhere.¹² Here we give a more detailed analysis of the BW_8 spectra, present and analyze the calculated structures and vibrational frequencies, and extend our experimental work to include the analogous spectra of B_2W_8 . Through comparison with calculated vibrational frequencies and infrared intensities, we have assigned the carriers of the observed spectra as the S_4 and D_{2d} symmetry cubic water octamers of BW_8 and B_2W_8 . The calculations provide a basis for determining the effect of benzene on the spectral signatures of the cubic $W_8(S_4)$ and $W_8(D_{2d})$.

II. METHODS

A. Experiment

The experimental apparatus employed in this work has been described previously.⁶² Cold, gas-phase B_mW_n clusters were produced by supersonically expanding a mixture of benzene and water vapor in Ne-70 (70% neon and 30% helium) from a pulsed valve of 0.8 mm diam operating at 20 Hz. The cluster size distribution formed in the expansion was controlled by adjusting metered flows of Ne-70 over the room temperature, liquid samples. Typical sample concentrations in the expansion were 0.3%–0.8% benzene, and 0.4%–1.0% water in a balance of Ne-70 at a total pressure of 2 bar.

B_mW_n clusters were resonantly ionized by the output of a Nd:YAG-pumped (Continuum, Powerlite 7020 series), doubled-dye (Lumonics, Hyper-Dye 500) laser operating at 20 Hz. The tunable output (0.4–1.3 mJ/pulse) was propagated through the ion source of the TOFMS in a 1 mm diam, collimated beam. One-color R2PI spectra were taken by gating around the arrival times of BW_n^+ clusters ($n=5-8$) and recording the integrated ion intensity present in those gates as a function of laser wavelength, using a digital oscilloscope (LeCroy 9400) interfaced to a personal computer.

UV–UV hole-burning spectroscopy was used to dissect the R2PI spectrum in a given mass channel into sub-spectra due to individual species. To that end, the output of an excimer-pumped doubled-dye laser was used to remove a significant fraction of the population from a selected ground state by setting its wavelength to a chosen feature in the R2PI spectrum with power sufficient to partially saturate the chosen transition (0.6–1.8 mJ UV/pulse). A second UV laser crossed the molecular beam 1 cm downstream from the first and was delayed in time by 12 μ s. This laser was tuned through the R2PI spectrum while the difference in ion signal from the probe laser with and without the hole-burning laser present was recorded. Transitions sharing the same ground state as the one probed by the hole-burning laser were detected as depletions in the ion signal.

RIDIR spectra in the OH stretch region were recorded using a method similar to that described previously.^{4,12,47,58} The pulsed, near-IR output (1.5 cm^{-1} resolution) of a Nd:YAG-pumped LiNbO₃ optical parametric oscillator (OPO)⁵⁸ was spatially overlapped with the UV laser used for R2PI, but preceding it in time by about 200 ns. With the UV laser fixed on a selected cluster's $S_1 \leftarrow S_0$ 6_0^1 transition (due to the benzene molecule in the cluster), the ion signal in the mass channel of interest was monitored as a function of OPO wavelength. Any infrared absorption occurring out of the same ground state as that monitored in R2PI was detected as a depletion in ion signal. In contrast to previous studies, the RIDIR spectra reported here were taken using active baseline subtraction (ABS). By firing the pulsed valve and UV laser at 20 Hz and the IR laser at 10 Hz, a gated integrator (Stanford Research Systems) recorded the difference in ion signal between alternating UV laser pulses, one with and one without the infrared light present.

B. Theory

Over the past few years, considerable progress has been made in developing a good understanding of the strengths and weaknesses of various theoretical methods for describing hydrogen-bonded systems. It is now clear that inclusion of electron correlation and the use of sufficiently flexible basis sets are essential for such studies. Both the MP2 (second-order Moller–Plesset) method and density functional theory (DFT), particularly when used with the Becke3LYP (LYP: Lee, Yang, Parr) functional,^{65–67} have been found to be quite useful for calculating structures and OH stretch vibrational frequencies of small water and methanol clusters^{68–72} and BW_n clusters with $n=1-3$.⁷³ MP2 calculations of the structures and vibrational frequencies of BW_8 would be computationally prohibitive, and, for this reason, we have used the Becke3LYP density functional method in this study. Prior studies⁷³ have shown that Becke3LYP calculations give structures and OH stretch frequency shifts for W_n and BW_n close to the corresponding MP2 results.

The majority of the calculations made use of a “mixed” basis set-6-31G(*d*)^{67,74} on the benzene and 6-31+G(*d*)^{67,74,75} on the water molecules. This mixed basis set, denoted 6-31+G(*d*)/6-31G(*d*) to indicate the greater flexibility on the water portion, supersedes the 6-31+G[*d,p*]/6-31G(*d*) basis set used in our earlier, preliminary report on BW_8 .¹² This switch in basis sets is motivated by the finding that Becke3LYP calculations with the 6-31+G(*d*) basis set more closely reproduce the experimentally observed trends in the OH stretch frequencies of small water clusters than do Becke3LYP calculations with the 6-31+G[*d,p*] basis set. Limited results obtained using the 6-31+G(*d*) basis set on both the water and benzene molecules are also reported.

Density functional methods are generally less sensitive to the atomic basis set than is the MP2 method.⁷⁶ Indeed, for W_2 , W_3 , and W_4 we have found Becke3LYP calculations with the 6-31+G(*d*) basis set give OH stretch frequencies very close to those obtained from Becke3LYP calculations with the much larger 6-311++G(2*df*,2*pd*) basis set.⁷⁷

The geometry optimizations on the D_{2d} and S_4 , W_8 clusters were carried out exploiting their symmetries. However, the optimizations of the corresponding BW_8 clusters were carried out in the absence of any constraints. The vibrational frequencies of the optimized structures were calculated in the harmonic approximation by use of analytical second derivatives. The electronic structure calculations were performed with the GAUSSIAN 94 program package.⁷⁸

As is well known, finite basis set calculations on weakly bonded species are subject to basis set superposition error (BSSE),⁷⁹ which tends to cause binding energies to be overestimated. In this study we make use of the standard counterpoise procedure⁷⁹ in order to obtain the BSSE correction to the binding energy of benzene to W_8 as well as for the total binding energy for $W_8(D_{2d})$. Since the BSSE corrections for $W_8(D_{2d})$ and $W_8(S_4)$ are anticipated to be nearly identical, the corresponding BSSE corrections for $W_8(S_4)$ were not carried out.

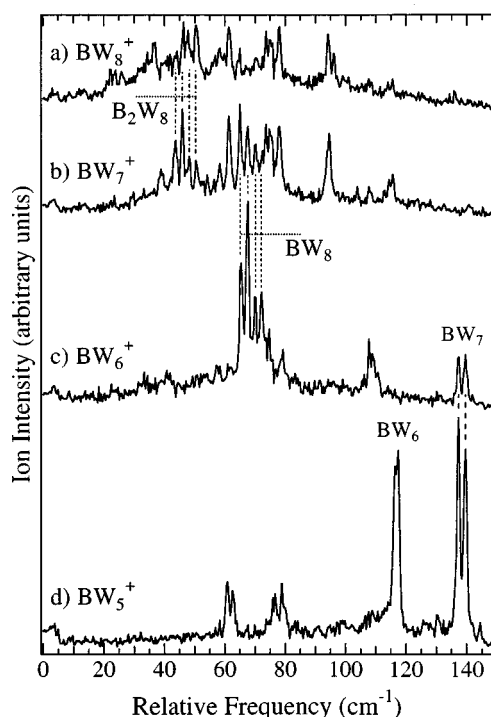


FIG. 2. One-color R2PI spectra of $B_m W_n$ clusters near the $S_1 \leftarrow S_0$ 6_0^1 transition of benzene, monitoring the BW_n^+ ions with (a) $n=8$, (b) $n=7$, (c) $n=6$, and (d) $n=5$. The zero of the frequency scale is the vibronically allowed 6_0^1 transition of the benzene monomer ($38\,609\text{ cm}^{-1}$). The labels denote transitions assigned to BW_6 , BW_7 , BW_8 , and B_2W_8 clusters.

III. RESULTS AND ANALYSIS

A. R2PI spectra

One-color R2PI spectra were recorded in the 6_0^1 (Fig. 2) and origin (Fig. 3) regions of the $S_1 \leftarrow S_0$ transition of benzene. Scans monitoring the BW_n^+ mass channels with $n=5-8$ are shown in Figs. 2(a)–2(d) and 3(a)–3(d), respectively. The 6_0^1 frequency shifts, 6_0^1 splittings, and relative origin to 6_0^1 intensities for these clusters are given in Table I. Vibronic frequency shifts for the clusters are reported with respect to either the 6_0^1 ($38\,609\text{ cm}^{-1}$) or 0_0^0 ($38\,086\text{ cm}^{-1}$) transitions of the benzene monomer. The spectra of Figs. 2 and 3 differ from those published in previous work⁶³ primarily in using 70% Ne in helium as carrier gas rather than helium. The assignments of the BW_6 and BW_7 transitions in the BW_5^+ and BW_6^+ mass channels are those deduced in earlier work.⁶³ R2PI spectra acquired in the 6_0^1 region (Fig. 2) differ from those taken at the origin region (Fig. 3) in several ways. First, each transition in the origin region is split into a doublet at 6_0^1 due to the loss of degeneracy in $\nu_6(e_{2g})$ induced by complexation to W_n . Second, the 6_0^1 transitions of the clusters are over an order-of-magnitude more intense than the origin transitions since intensity at the electric-dipole-forbidden origin is only weakly induced by the symmetry-breaking effects of individual water clusters on benzene. Third, fragmentation of the BW_n clusters following photoionization is greater at 6_0^1 than at the origin, reflecting the extra 1040 cm^{-1} of energy which could be imparted to the cluster in the one-color R2PI process.

Previous R2PI studies on smaller BW_n clusters,^{62,63}

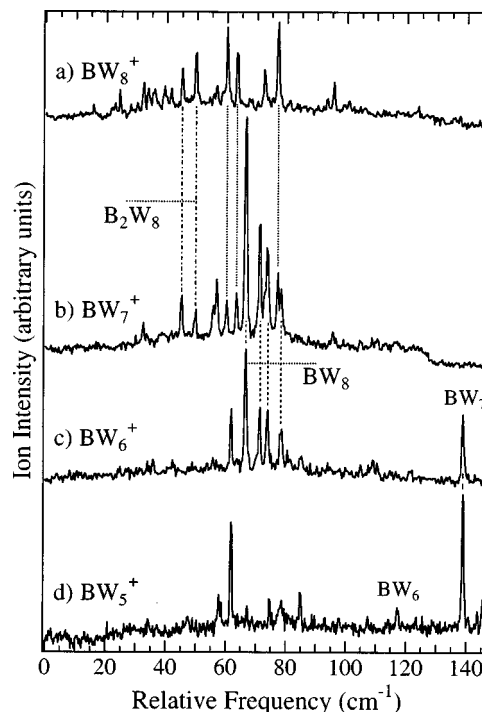


FIG. 3. One-color R2PI spectra of $B_m W_n$ clusters near the $S_1 \leftarrow S_0$ origin transition of benzene, monitoring the BW_n^+ ions with (a) $n=8$, (b) $n=7$, (c) $n=6$, and (d) $n=5$. The zero of the frequency scale is the dipole-forbidden 0_0^0 transition of the benzene monomer ($38\,086\text{ cm}^{-1}$). The clusters gain intensity by the symmetry-breaking effect of W_n on benzene. The labels denote transitions assigned to BW_6 , BW_7 , BW_8 , and B_2W_8 clusters. The transitions joined by dotted lines (\cdots) in BW_7^+ and BW_8^+ are tentatively assigned to BW_9 , and will be discussed elsewhere (Ref. 85). See the text for further discussion.

benzene-(methanol)_m clusters,⁸⁰ mixed benzene-(water)_n-(methanol)_m clusters,⁸¹ and indole- W_n clusters⁸² have shown that fragmentation of the neutral clusters following photoionization by loss of one or more water or methanol molecules can occur, complicating the assignment of a set of transitions in a particular mass channel to a given neutral cluster size. Figure 4 displays histograms of the amount of fragmentation occurring in one-color R2PI studies of BW_n clusters with $n=1-9$. For clusters with up to five water molecules, there is efficient fragmentation by loss of a single water molecule. In

TABLE I. One-color resonant two-photon ionization data for $B_m W_n$ clusters.

Cluster	Relative frequency ^a (cm^{-1})	6_0^1 Splitting ^c (cm^{-1})	$0_0^0/6_0^1$ Intensity ratio %
BW_6	117 ^b	d	0.5 ^e
BW_7	138 ^b	2.3	2 ^e
$BW_8(I)$	66	2.2	5
$BW_8(II)$	71	2.2	4
$B_2W_8(I)$	45	2.2	2.5
$B_2W_8(II)$	50	2.2	3

^aFrequency shift relative to 6_0^1 transition of C_6H_6 ($38\,609\text{ cm}^{-1}$).

^bResults from previous work (Ref. 39).

^cSplittings are to $\pm 0.3\text{ cm}^{-1}$.

^dNo 6_0^1 splitting resolvable with the present laser system.

^eSet at the upper limit established for this ratio in Ref. 61.

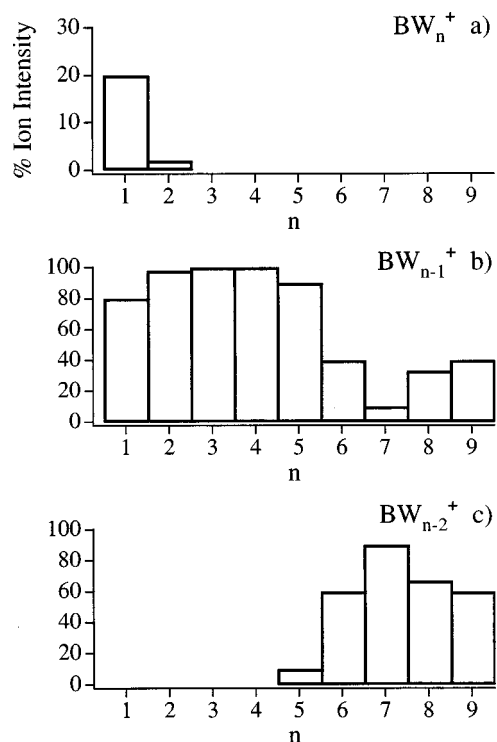


FIG. 4. Fragmentation of BW_n clusters into the mass channels: (a) BW_n^+ , (b) BW_{n-1}^+ , and (c) BW_{n-2}^+ after one-color resonant two-photon ionization via the BW_n 6_0^1 transitions. Smaller BW_n clusters ($n \leq 5$) efficiently fragment, losing one water molecule following photoionization. The loss of a second water molecule becomes energetically favorable at BW_6 and continues for larger clusters.

fact, BW_1 and BW_2 are the only clusters with measurable ion signal in the parent mass channel.^{62,63,83} In BW_6 and BW_7 , loss of a second water molecule also is observed, suggesting that an energetic threshold to this process is being reached at $n=6$. This additional fragmentation in BW_6 and larger clusters accompanies the change over from cyclic water sub-structures in smaller BW_n clusters to three-dimensional H-bonded networks in BW_n with $n \geq 6$.^{4,47,84}

The efficient fragmentation of the clusters following photoionization arises because the ionized cluster has a very different lowest-energy structure than the π H-bonded structure taken up by the neutral.⁸⁵ The Franck–Condon factors to the adiabatic ionization threshold are then very poor, hindering two-color R2PI and producing ionized clusters with substantial internal energy, which can subsequently fragment.

If BW_8 clusters fragment similarly to BW_6 and BW_7 upon photoionization, then they will lose either one or two water molecules and appear in both the BW_7^+ and BW_6^+ mass channels, respectively. The R2PI spectra at the origin [Figs. 3(b) and 3(c)] identify four transitions 66.5, 71.3, 73.8, and 78.2 cm^{-1} above the $S_1 \leftarrow S_0$ origin of benzene which appear only in the BW_6^+ and BW_7^+ mass channels. These spectra have benzene concentration dependences similar to other single-benzene clusters, and are thereby assigned to BW_8 . The single transition at +61.8 cm^{-1} which appears in the BW_6^+ and BW_5^+ mass channels [Figs. 3(c) and 3(d)] is tentatively assigned to a second isomer of BW_7 . Further discussion of this species will be taken up elsewhere.⁸⁶

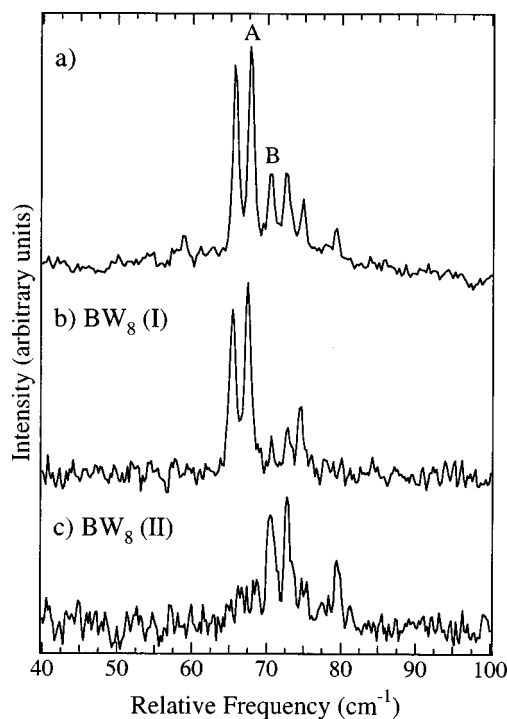


FIG. 5. (a) One-color R2PI spectrum in the 6_0^1 region of $S_1 \leftarrow S_0$ transition of BW_8 , recorded while monitoring the BW_6^+ mass channel. BW_8 transitions were detected in BW_6^+ due to photoionization-induced fragmentation of two water molecules. (b) and (c): Ultraviolet hole-burning spectra of transitions assigned to BW_8 . The hole-burning laser was tuned to transitions A (67.6 cm^{-1}) and B (70.3 cm^{-1}) in recording the spectra in (b) and (c), respectively.

As the concentration of benzene in the expansion was increased from 0.3% [Fig. 2(b) BW_7^+] to 0.6% [Fig. 6(a) BW_7^+], several transitions grew in intensity relative to those assigned to B_1W_n species. Two of these transitions, at +45.1 and +49.8 cm^{-1} , show a similar spacing and intensity profile to the most intense transitions assigned to BW_8 , but are shifted about 20 cm^{-1} to the red [Fig. 3(b)]. These transitions appear primarily in the BW_7^+ and BW_8^+ mass channels, but also are observed in the $B_2W_6^+$ mass channel and are thereby assigned to the B_2W_8 cluster. The appearance of the B_2W_8 transitions in the BW_7^+ and BW_8^+ mass channels indicates that, with two benzene molecules present in the cluster, fragmentation following photoionization typically involves loss of a benzene molecule either with or without water loss, respectively. It is not surprising that benzene would be selectively lost from the photoionized cluster, since the least strongly bound molecule in the B_2W_8 cluster will be the neutral benzene if the positive charge is localized on the other benzene molecule. As we will see shortly, the hole-burning and RIDIR spectra provide a further basis for this assignment.

B. UV–UV hole-burning spectra

1. BW_8 isomers

UV–UV hole-burning spectra collected in the BW_6^+ mass channel in the 6_0^1 region of benzene are shown in Figs. 5(b) and 5(c). The BW_6^+ R2PI spectrum of Fig. 5(a) marks the transitions used for hole burning as A and B. The R2PI

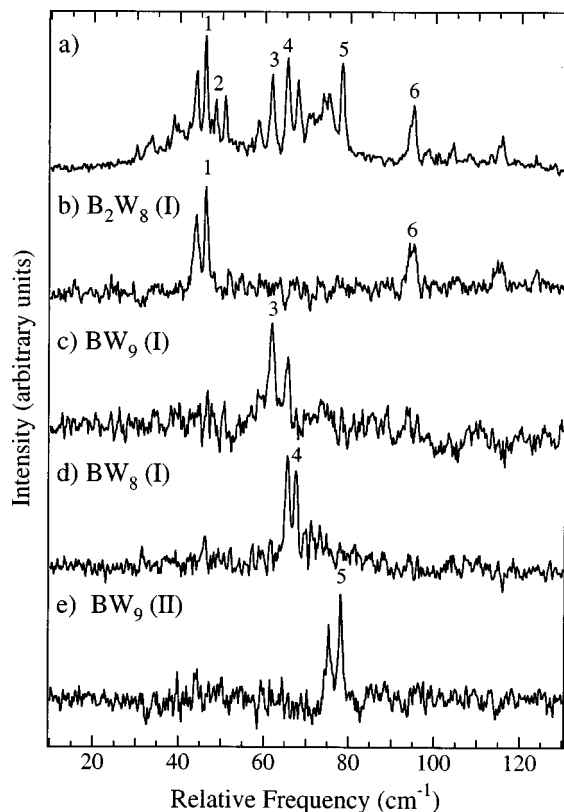


FIG. 6. (a) One-color R2PI spectrum monitoring the BW_7^+ mass channel. (b)–(e): Hole-burning spectra taken with the hole-burning laser tuned to transitions 1, 3, 4, and 5, located (b) 46.1 cm^{-1} , (c) 61.7 cm^{-1} , (d) 67.6 cm^{-1} , and (e) 78.1 cm^{-1} above the 6_0^1 transition of benzene monomer. The assignments of the transitions to BW_n clusters are given. See the text for further discussion.

transitions assigned in Sec. III A to BW_8 cleanly divide under hole burning into two sub-spectra, indicating that there are two isomers of BW_8 present. The spectrum of each isomer consists of a doublet [centered at $+66.5\text{ cm}^{-1}$ for $BW_8(I)$ and at $+71.4\text{ cm}^{-1}$ for $BW_8(II)$] and a weaker second doublet 7 cm^{-1} to the blue, tentatively assigned as a combination band involving a low-frequency intermolecular vibration.

The ultraviolet (UV) spectra of the BW_8 isomers suggests that the isomers are close structural analogs of one another. First, the frequency shifts differ only by 4.9 cm^{-1} out of $\sim 38\,000\text{ cm}^{-1}$. Second, the identical 6_0^1 splittings (2.2 cm^{-1}) indicate that in both isomers the W_n entity induces similar asymmetry in the benzene molecule. Third, the isomers show the same intermolecular structure. Finally, the isomers fragment with similar efficiencies into the BW_6^+ and BW_7^+ mass channels.

Yet, while the spectra of the two isomers are very similar, they are quite different from those of BW_6 and BW_7 , implying that the BW_8 species are structurally distinct from BW_6 and BW_7 . The $S_1 \leftarrow S_0$ electronic frequency shifts for the BW_8 isomers ($+66.5$ and $+71.4\text{ cm}^{-1}$) are much less than those for BW_6 ($+117\text{ cm}^{-1}$) and BW_7 ($+138\text{ cm}^{-1}$) clusters. Furthermore, the extent of fragmentation following photoionization (Fig. 4) decreases in going from BW_7 to BW_8 . Such a reduction is consistent with a W_8 H-bonded

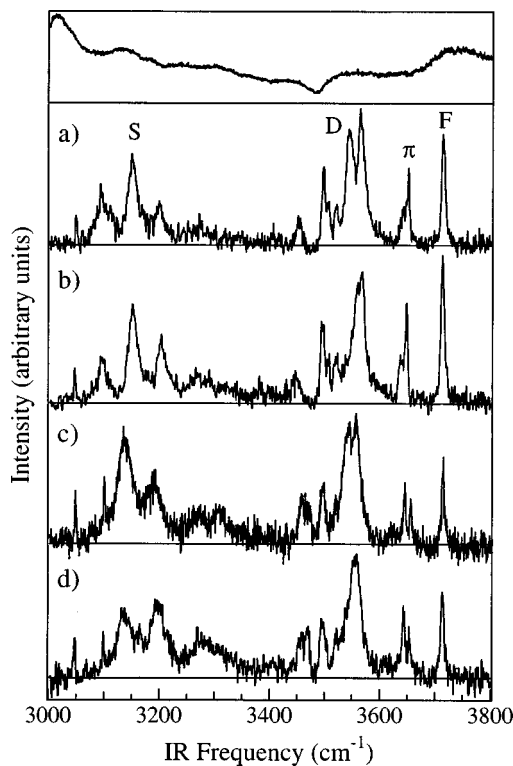


FIG. 7. Resonant ion-dip infrared spectra of (a) $BW_8(I)$, (b) $BW_8(II)$, (c) $B_2W_8(I)$, and (d) $B_2W_8(II)$ isomers. The monitored transitions for $BW_8(I)$ and $BW_8(II)$ are labeled *A* and *B* in Fig. 5, while those for $B_2W_8(I)$ and $B_2W_8(II)$ are labeled 1 and 2 in Fig. 6, respectively. The top trace is the OPO power curve for the LiNbO_3 crystal used in this study. The spectra have not been corrected for OPO power.

structure in BW_8 which is more stable than the corresponding W_7 structure in BW_7 , and thereby less easily broken apart following photoionization.

2. B_2W_8 isomers

UV–UV hole-burning spectra collected in the BW_7^+ mass channel near the 6_0^1 transition of benzene are shown in Figs. 6(b)–6(e). The corresponding R2PI spectrum of this mass channel is shown in Fig. 6(a) for comparison. The hole-burning spectra of Figs. 6(b)–6(e) are recorded with the ultraviolet hole-burning laser tuned to transitions 1, 3, 4, and 5, respectively. Each of these transitions produces a hole-burning spectrum due to a unique species each of which strongly favors $\Delta v = 0$ Franck–Condon factors in the intermolecular modes. Transitions in the hole-burning spectra of Figs. 6(c) and 6(e) are assigned as isomers of the BW_9 cluster and will be discussed elsewhere.⁸⁶ The hole-burning spectrum shown in Fig. 6(d) is assigned to the $+66.5\text{ cm}^{-1}$ isomer of BW_8 [i.e., $BW_8(I)$]. Hole-burning spectroscopy could not be fruitfully applied to the other BW_8 isomer in this mass channel due to its lower intensity and the nearby spectral congestion [Fig. 6(a)].

In the context of this paper, the two sets of doublets labeled 1 and 2 are of most consequence. These are the 6_0^1 transitions built on the origin transitions assigned previously to B_2W_8 in Figs. 3(a) and 3(b). The hole-burning spectrum recorded with the hole-burning laser tuned to transition 1

TABLE II. Experimental vibrational frequencies,^a widths,^b and integrated intensities^c for the conformational isomers of BW₈ and B₂W₈.

H-bonded topology of [BW ₈] and {B ₂ W ₈ }	Number of OH groups	I[BW ₈ (S ₄)]			II[BW ₈ (D _{2d})]			I[B ₂ W ₈ (S ₄)]			II[B ₂ W ₈ (D _{2d})]		
		Freq.	(Width)	Int.	Freq.	(Width)	Int.	Freq.	(Width)	Int.	Freq.	(Width)	Int.
Free OH	[3], {2}	3713	(7)	3	3713	(7)	3	3714	(5)	2	3713	(7)	2
π H-bonded OH	[1], {2}	3650	(6)	4	3649	(6)	4	3656	(5)	4	3653	(5)	4
		3642	(8)		3637	(8)		3645	(5)		3643	(6)	
Double-donor OH	8												
Asymmetric stretch				29			20			28			18
		3563	(20)		3568	(25)		3557	^d		3555	(30)	
		3543	(20)					3545	^d				
Symmetric stretch				12			12			18			16
		3520	(9)		3523	(13)		3520	(~8)		3522	(8)	
		3506	(~8)		3508	(~8)		3495	(11)		3496	(12)	
		3496	(8)		3497	(9)		3468	(12)		3470	(10)	
		3454	(10)		3446	(12)		3458	(11)		3458	(12)	
Single-donor OH	4			16			18			24			17
		3198	(~20)		3203	(19)		3190	(32)		3198	(25)	
		3148	(20)		3151	(21)		3135	(33)		3137	(31)	
		3092	(20)		3097	(16)							
CH stretch region of benzene				~0.6			~0.6			~1.3			~1.0
		3048	(4)		3047	(4)		3100	(3)		3099	(3)	
								3048	(3)		3047	(3)	

^aAll frequencies reported in wave numbers (cm⁻¹).

^bThe widths (in cm⁻¹) of the transitions are full-widths at half-maximum.

^cApproximate power-normalized, integrated intensities for each type of OH stretch. The BW₈/B₂W₈ free OH intensities are scaled to values of 3.0/2.0, since there are 3/2 free OH groups present in the BW₈/B₂W₈ isomers, respectively. The intensities have not been corrected for the effects of partial saturation.

^dTransitions were unresolved at the resolution of the OPO system (2 cm⁻¹).

[Fig. 6(b)] indicates that, as with BW₈, the set of four transitions assigned to B₂W₈ is composed of two doublets due to two different B₂W₈ isomers. The spectrum of Fig. 6(b) also identifies transition 6 at 95 cm⁻¹ to the same B₂W₈ isomer responsible for transition 1. The former transition could be an intermolecular transition built on the ν_0^1 band. More likely, however, is an assignment as the second ν_0^1 transition arising from the presence of two benzene molecules in the B₂W₈(I) isomer. Transitions 1 and 2 in B₂W₈ possess the same relative spacing (4.7 cm⁻¹), ν_0^1 splitting (2.2 cm⁻¹), and relative intensity as the transitions due to the two BW₈ isomers. This suggests a structural similarity between the BW₈ and B₂W₈ clusters.

C. RIDIR spectra

Overview RIDIR spectra of the BW₈ and B₂W₈ isomers in the OH and CH stretch region of the infrared are shown in Figs. 7(a)–7(d). The RIDIR spectra of the two isomers of BW₈ [Figs. 7(a) and 7(b)] were obtained by monitoring the BW₆⁺ mass channel with the R2PI laser tuned to transitions A and B, respectively, of Fig. 5. The analogous transitions in B₂W₈ [1 and 2 in Fig. 6(a)] were used to record the RIDIR spectra of Figs. 7(c) and 7(d), respectively, while monitoring the BW₇⁺ ion signal. The frequencies, full width at half maximum (FWHM), and approximate power-normalized, integrated intensities for each kind of OH stretch vibration are given for the four species in Table II. The OH stretch absorptions in Fig. 7 can be grouped into one of four categories: (i) The free (nonbonded) OH stretch transitions appearing around 3715 cm⁻¹ marked by an F, (ii) the π H-bonded

OH stretch of the water molecule which is complexed to benzene's π cloud, shifted down in frequency by the weak π H-bond to about 3650 cm⁻¹, (iii) the double-donor (H₂O–H₂O) H-bonded OH stretches in the 3450–3600 cm⁻¹ region (D), and (iv) the single-donor (H₂O–H₂O) H-bonded OH stretches in the 3100–3250 cm⁻¹ region (S). The CH stretch fundamentals of the benzene molecule(s) in the cluster appear as a Fermi resonance triad at 3048, 3074, and 3100 cm⁻¹, essentially unshifted from their values in free benzene.

The simplicity and striking similarities of the IR spectra of Fig. 7 suggests that a common H-bonding topology is shared by the water molecules in these clusters. In the two isomers of BW₈, the most significant difference is found in the double-donor region near 3550 cm⁻¹, where there are two resolved, intense bands in Fig. 7(a) and only one in Fig. 7(b). This difference is a distinguishing signature for the two isomers. A more subtle difference is found in the single-donor region, where the highest-frequency single-donor band is more intense in Fig. 7(b) than in Fig. 7(a).

A comparison of the RIDIR spectra of the two isomers of BW₈ with those previously reported^{4,47} for BW₆ and BW₇ shows the BW₈ spectra to be surprisingly simple. The BW₆ and BW₇ clusters are the smallest BW_n clusters which possess a three-dimensional H-bonded network containing double-donor water molecules. In both BW₆ and BW₇, the distinction between double-donor and single-donor bands is blurred, with transitions appearing throughout the region from 3600 to 3000 cm⁻¹. In both isomers of BW₈, by contrast, the single-donor transitions appear between 3050 and

3200 cm^{-1} , leaving a 300 cm^{-1} gap between double-donor and single-donor transitions. Furthermore, the double-donor regions of BW_6 and BW_7 have a series of similar-intensity bands, unlike the present BW_8 spectra, which are dominated by the bands at 3550 cm^{-1} . As we shall see shortly, the apparent simplicity of the BW_8 infrared spectra reflects the high symmetry of the W_8 structure in the cluster.

The RIDIR spectra of the two B_2W_8 isomers [Figs. 7(c) and 7(d)] bear a strong resemblance to their BW_8 counterparts [Figs. 7(a) and 7(b), respectively], suggesting that the same hydrogen-bonding topology is taken up by the W_8 cluster in B_2W_8 as in BW_8 . Like the BW_8 spectra, the OH stretch fundamentals of B_2W_8 divide cleanly into well-defined sub-groups involving free, π H-bonded, double-donor, and single-donor OH vibrations. The double-donor regions of B_2W_8 and BW_8 are especially similar, with Fig. 7(c) exhibiting the same intense doublet as Fig. 7(a), and Fig. 7(d) the same unresolved single feature as found in Fig. 7(b).

The free and π H-bonded OH stretch regions show most directly the effects of the second benzene molecule. In both Figs. 7(c) and 7(d), the addition of the second benzene increases the intensity of the C–H stretch fundamentals (3048 and 3100 cm^{-1}), consistent with the assignment to B_2W_8 . At the same time, by comparison to the BW_8 spectra, the B_2W_8 spectra swap intensity in the free OH stretch region in favor of an additional band in the π H-bonded OH region. It would seem a firm conclusion, then, that the second benzene π H-bonds to another of the free OH groups in the W_8 sub-cluster. Finally, the single-donor region of the B_2W_8 isomers' spectra differs from their BW_8 counterparts in shifting the absorptions in such a way that only two resolved bands are now observed, with the highest frequency band more intense in Fig. 7(d) than in Fig. 7(c).

D. Theoretical results

1. Structures and binding energies

The computed lowest-energy structures for the D_{2d} and S_4 forms of W_8 and their complexes with benzene are shown in Fig. 8. Their key structural parameters are given in Table III, while Table IV reports their dipole moments, rotational constants, and binding energies. Unless noted otherwise, this discussion will focus on the results obtained with the 6-31+G(d)/6-31G(d) basis set. The atom numbering scheme used in Table III is given in Fig. 8. Additional material about the structures of W_8 and BW_8 are found in E-PAPS form.⁸⁷

In agreement with earlier theoretical studies,^{8,13,16,17,20} the D_{2d} and S_4 forms of W_8 are found to be nearly isoenergetic (Table IV), with the D_{2d} form being predicted to be about 0.06 kcal/mol more stable than the S_4 form in the absence of corrections for vibrational zero point energy (ZPE), but with the S_4 form being more stable by 0.11 kcal/mol when ZPE corrections are included. The ZPE's were calculated using the computed harmonic vibrational frequencies.⁸⁷

Both the S_4 and D_{2d} BW_8 isomers [Figs. 8(c) and 8(d), respectively] have calculated minimum-energy structures in which benzene attaches to the W_8 cube via a π H-bond which distorts, but does not break up, the cubic H-bonding network. The distortion induced by benzene is greatest in the

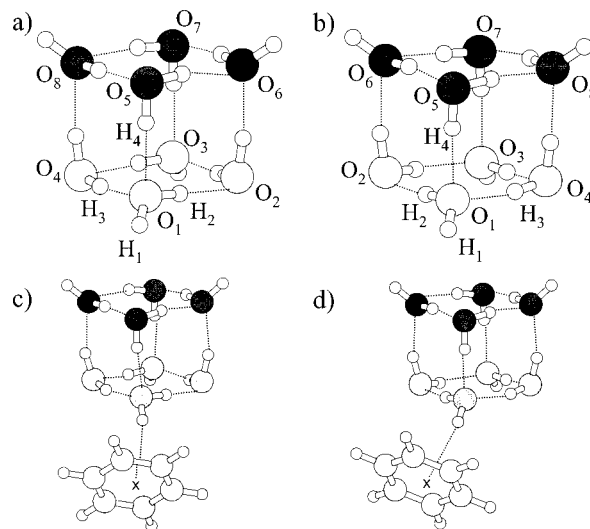


FIG. 8. Calculated [Becke3LYP/6-31+G(d)/6-31G(d)] minimum-energy structures for the S_4 (a) and D_{2d} (b) water octamers and the corresponding BW_8 clusters (c) and (d), respectively.

vicinity of the water molecule bonded to the ring. In particular, the water to which the benzene is attached becomes a better OH acceptor (shrinking the O–O distances by about 0.030 Å) and poorer OH donor (increasing the O–O distance by about the same amount) as a result of the interaction with the benzene ring.⁸⁷

The interaction energy between benzene and W_8 in BW_8 is calculated to be nearly the same (to within 0.02 kcal/mol) in the $\text{BW}_8(D_{2d})$ and $\text{BW}_8(S_4)$ isomers, both with and without inclusion of the counterpoise correction [and with both the 6-31+G(d)/6-31+G(d) and 6-31+G(d)/6-31G(d) basis sets]. With inclusion of vibrational ZPE, the $\text{BW}_8(S_4)$ isomer is predicted to be slightly (~ 0.05 kcal/mol) more

TABLE III. Key structural data for the S_4 and D_{2d} isomers of W_8 and BW_8 ^a From Becke3LYP calculations.^b

	S_4		D_{2d}	
	W_8	BW_8	W_8	BW_8
$R(\text{O}_2\text{--O}_1)$	2.676	2.702	2.680	2.706
$R(\text{O}_4\text{--O}_1)$	2.843	2.815	2.837	2.810
$R(\text{O}_5\text{--O}_1)$	2.839	2.809	2.837	2.807
$r(\text{O}_1\text{--H}_2)$	1.004	0.999	1.004	0.999
$r(\text{O}_4\text{--H}_3)$	0.982	0.985	0.982	0.985
$r(\text{O}_5\text{--H}_4)$	0.982	0.985	0.982	0.984
$r(\text{O}_1\text{--H}_1)$	0.969	0.973	0.969	0.973
$r(\text{X--H}_1)^c$		2.535		2.537
$r(\text{X--O}_1)^c$		3.460		3.465
$\theta(\text{O}_1\text{--H}_2\cdots\text{O}_2)$	167.26	165.02	167.41	165.15
$\theta(\text{O}_1\cdots\text{H}_3\text{--O}_4)$	159.34	160.39	159.50	160.01
$\theta(\text{O}_1\cdots\text{H}_4\text{--O}_5)$	160.19	161.77	159.50	160.94
$\theta(\text{O}_4\text{--O}_1\text{--O}_2)$	88.38	88.81	88.50	88.83
$\theta(\text{O}_4\text{--O}_1\text{--O}_5)$	86.31	87.21	87.46	88.52
$\theta(\text{O}_2\text{--O}_1\text{--O}_5)$	89.54	90.16	88.50	89.04
$\theta(\text{O}_1\text{--O}_2\text{--O}_3)$	91.56	90.56	91.44	90.52

^aBond lengths are in Angstroms, angles in degrees. See Fig. 8 for numbering scheme.

^bResults obtained with the mixed 6-31+G(d)/6-31G(d) basis set.

^cX is the inversion center of the benzene ring.

TABLE IV. Energetics and properties of the S_4 and D_{2d} isomers of W_8 and BW_8 .^a

	S_4		D_{2d}	
	W_8	BW_8	W_8	BW_8
Binding energy ^b (kcal/mol)	-88.0	-3.84	-88.1(-74.2)	-3.83
BSSE (kcal/mol) ^c	14.6	1.43	14.6(7.5)	1.62
Corrected ^c binding energy (kcal/mol)	-73.3	-2.41	-73.4(-66.7)	-2.21
Dipole moment (Debye)	0.000	1.236	0.000	1.167
Rotational constants (GHz)	0.9093	0.6815	0.9099	0.6847
	0.8829	0.2127	0.9099	0.2165
	0.8829	0.2120	0.8580	0.2139

^aAll results, except those in parentheses are obtained from Becke3LYP/6-31+G(*d*) calculations using the mixed 6-31+G(*d*)/6-31G(*d*) basis set. The results in parentheses for the D_{2d} form of W_8 are obtained from single-point calculations using the 6-31++G(*d,p*) basis set at the 6-31+G(*d*) optimized geometries.

^bBinding energy of W_8 calculated from $W_8 \rightarrow 8W_1$ and that for BW_8 for $BW_8 \rightarrow B+W_8$.

^cCorrected for basis set superposition error (BSSE) using the counterpoise method.

stable than the $BW_8(D_{2d})$ isomer. Obviously, Becke3LYP/6-31+G(*d*) calculations are not reliable for predicting relative energies correct to hundredths of a kcal/mol, even for two such structurally similar isomers. It is clear, however, that the two low-energy BW_8 isomers, like the W_8 isomers from which they derive, are nearly isoenergetic.⁸⁷

2. Vibrational spectra

Figure 9 and Table V summarize the calculated OH stretch spectra for the S_4 and D_{2d} forms of W_8 [Figs. 9(a) and 9(c)] and BW_8 [Figs. 9(b) and 9(d)]. In discussing these results, use will be made of the frequency shifts obtained by subtracting the mean of the harmonic frequencies (3792.2 cm^{-1}) of the symmetric and antisymmetric stretch modes of the water monomer (calculated at the same level of theory) from the calculated OH stretch frequencies of the W_8 and BW_8 species.^{4,11,88}

As anticipated from the structures, the OH stretch frequencies of the S_4 and D_{2d} forms of W_8 separate into three regions associated with vibrations of the free OH, single-donor OH, and double-donor OH groups. Analysis of the normal modes indicates that this separation is near complete, with greater than 98% of the OH stretch amplitude isolated on the OH groups of the indicated type. Due to the high symmetry of the W_8 structures, the normal modes are completely delocalized over the OH groups of a given type, with each vibration differing from the others in its class in the relative phases of the oscillations of the OH groups. The four free OH vibrations have small ($\sim 18 \text{ cm}^{-1}$) frequency shifts, are nearly degenerate, and have low IR intensities. The four single-donor OH stretch modes, with their strong, linear H-bonds, have large frequency shifts (-578 to -674 cm^{-1}). In the D_{2d} isomer, it is the highest-frequency single-donor mode, which is nondegenerate, which carries all the infrared

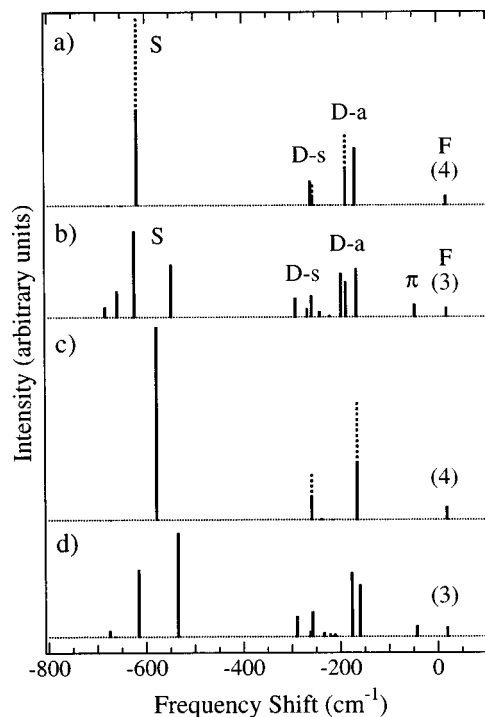


FIG. 9. Calculated [Becke3LYP/6-31+G(*d*)/6-31G(*d*)] OH stretch vibrational frequency shifts and infrared intensities for the S_4 water octamer (a), the S_4 water octamer in BW_8 (b), the free D_{2d} water octamer (c), and the D_{2d} water octamer in BW_8 (d). The zero of the frequency scale is the mean of the symmetric and antisymmetric OH stretch modes of the water monomer calculated at the same level of theory (3792.2 cm^{-1}). The normal modes separate into groups as free OH (F), π H-bonded OH (π), double-donor antisymmetric stretch (*D-a*), double-donor symmetric stretch (*D-s*), and single-donor (S).

intensity. In the S_4 isomer, the highest-frequency single-donor mode is doubly degenerate, but the pair of modes carries the same integrated intensity as its nondegenerate D_{2d} counterpart. The frequencies of these single-donor IR bands differ by 39 cm^{-1} , with the D_{2d} isomer (3214 cm^{-1}) higher in frequency than S_4 (3175 cm^{-1}). This difference serves as the basis for the distinction between the $W_8(D_{2d})$ and $W_8(S_4)$ isomers by Buck and co-workers⁴⁴ in their size-selected IR spectroscopy on W_8 .

The double-donor $W_8(S_4)$ and $W_8(D_{2d})$ vibrations appear with intermediate frequency shifts, ranging from -166 to -261 cm^{-1} (Table IV). The double-donor vibrations are shifted less than the single-donor OH stretch vibrations because of the weaker, nonlinear H-bonds created when both OH groups on a given water molecule are involved in H-bonds in a strained structure such as the cube. The result is a gap between single-donor and double-donor fundamentals of over 300 cm^{-1} [Figs. 9(a) and 9(c)]. The four highest-frequency transitions have antisymmetric stretch character on each of the double-donor water molecules (and are, therefore, hereafter labeled *D-a*), while the four lowest-frequency modes are nominally double-donor symmetric stretch in character (*D-s*). The double-donor *D-a* doublet in $W_8(S_4)$ is perhaps the most striking difference between the computed IR spectra of $W_8(S_4)$ and $W_8(D_{2d})$.⁸⁷

The calculations reveal that the addition of a benzene molecule to the $W_8(D_{2d})$ and $W_8(S_4)$ clusters has several

TABLE V. Comparison of the OH stretch vibrational frequencies (cm^{-1}) and shifts^a (cm^{-1}) of W_8 and BW_8 at the Becke3LYP level of theory.^b

D_{2d} Form						S_4 Form					
W_8			BW_8			W_8			BW_8		
Freq.	Shift ^a	Intensity ^c	Freq.	Shift ^a	Intensity ^c	Freq.	Shift ^a	Intensity ^c	Freq.	Shift ^a	Intensity ^c
3811.5	18.6	0	3812.0	19.1	50	3810.7	17.8	0	3811.4	18.5	53.3
3811.3	18.4	58	3811.6	18.7	71	3810.5	17.6	56	3810.9	18.0	59.9
3811.3	18.4	58	3810.9	17.9	63	3810.5	17.6	100	3810.7	17.8	70.1
3811.3	18.3	143	3749.2	-43.7	215	3810.5	17.6	100	3745.5	-47.4	257.0
3627.2	-165.8	1156	3632.4	-160.5	1021	3624.0	-168.9	1143	3626.3	-166.6	959.1
3627.2	-165.8	1156	3615.9	-177.0	1265	3605.1	-187.8	696	3604.6	-188.3	699.7
3577.5	-215.4	0	3580.3	-212.7	55	3605.1	-187.8	696	3595.0	-197.9	874.2
3577.5	-215.4	0	3570.5	-222.4	58	3575.0	-217.9	0	3571.5	-221.5	39.4
3553.5	-239.4	28	3558.2	-234.7	84	3549.1	-243.8	0	3550.7	-242.2	118.4
3550.9	-242.0	0	3534.5	-258.5	492	3537.1	-255.9	202	3534.6	-258.3	421.7
3533.4	-259.5	451	3529.9	-263.0	113	3537.1	-255.9	202	3525.3	-267.6	171.0
3533.4	-259.5	451	3502.4	-290.5	407	3532.2	-260.7	486	3500.6	-292.3	379.1
3214.0	-578.9	3811	3257.5	-535.4	2044	3175.3	-617.6	1847	3245.0	-547.9	1041.9
3146.3	-646.7	3	3176.5	-616.4	1327	3175.3	-617.6	1847	3168.9	-624.1	1694.6
3146.3	-646.7	3	3128.7	-664.3	8	3142.4	-650.5	4	3133.4	-659.5	527.2
3119.1	-673.8	0	3117.1	-675.8	130	3115.0	-678.0	0	3109.5	-683.4	212.5

^aVibrational frequency shifts are reported relative to the average of symmetric and asymmetric stretch frequencies of H_2O at the same level of theory (3792.2 cm^{-1} for the 6-31+G(*d*) basis set).

^bResults obtained using the 6-31+G(*d*) basis set on water and the 6-31G(*d*) basis set on benzene.

^cCalculated intensities are reported in units of km/mol .

important consequences for the OH stretch IR spectrum. The three of the free OH stretch modes not involved in π H-bonding are virtually unchanged from their values in W_8 . In contrast, the frequency of the OH π H-bonded to the benzene ring is shifted down in frequency by about 65 cm^{-1} relative to the frequencies of the free OH stretch modes of the bare W_8 clusters. Moreover, this mode is highly localized and has an intensity comparable to the sum of the remaining three free OH vibrations.

The minor distortions induced in the W_8 cubes by benzene produce normal modes with an unequal sharing of the vibrational amplitudes amongst the OH groups of a given type. Nevertheless, the modes retain their classification as double-donor or single-donor vibrations. The partial localization causes a splitting of the degenerate W_8 modes and induces infrared intensity in other vibrations which were previously forbidden (Fig. 9). Because benzene attaches to a single-donor water molecule, the single-donor region is most affected by these changes. In the double donor region, the degenerate *D-a* modes of $W_8(D_{2d})$ and $W_8(S_4)$ are split by benzene, but by only 17 and 9 cm^{-1} , respectively.⁸⁷

E. The comparison between experiment and theory

In order to compare with the experimental RIDIR spectra of the two isomers of BW_8 , the computed IR frequencies and intensities from Figs. 9(b) and 9(d) are given Gaussian widths which match the experimental widths of the OH stretch fundamentals. Figures 10(c) and 10(d) report the computed spectra for $BW_8(S_4)$ and $BW_8(D_{2d})$ including those widths, placed directly beneath the experimental spectra of Figs. 10(a) and 10(b) for comparison. The close correspondence between the computed and experimental spectra is immediately evident. Several aspects of the comparison argue for an assignment of the $BW_8(I)$ isomer responsible

for Fig. 10(a) as $BW_8(S_4)$ [Fig. 10(c)] and the $BW_8(II)$ isomer responsible for Fig. 10(b) as $BW_8(D_{2d})$ [Fig. 10(d)]. First, the computed spectra mirror the simplicity of the experimental spectra and their clean separation into free, π , double-donor and single-donor transitions, including the more than 300 cm^{-1} gap between single-donor and double-donor transitions. Neither the C_2 or C_i cubic W_8 structures nor any noncubic W_8 structures can reproduce these general features of the BW_8 spectra. Secondly, the computed spectra correctly reproduce the characteristic differences between the two isomers in the double-donor region. In particular, the spectrum calculated for $BW_8(S_4)$ [Fig. 10(c)] reproduces the experimental doublet in the *D-a* region of Fig. 10(a), while that for $BW_8(D_{2d})$ [Fig. 10(d)] possesses a single, unresolved *D-a* feature, as in Fig. 10(b). Third, the calculated spectra faithfully mirror the benzene-induced splittings observed in the single-donor region, including the greater intensity of the highest-frequency single-donor transition in Fig. 10(b) than in Fig. 10(a). On the basis of these considerations, we assign the spectrum of Fig. 10(a) to $BW_8(S_4)$ and that in Fig. 10(b) to $BW_8(D_{2d})$. The corresponding UV spectra for $BW_8(S_4)$ and $BW_8(D_{2d})$ are shown in the UV-UV hole-burning spectra of Figs. 5(b) and 5(c), respectively.

We have not carried out calculations on the B_2W_8 clusters due to the large CPU times which would have been required. However, the assignment of the two isomers of BW_8 as $BW_8(S_4)$ and $BW_8(D_{2d})$ suggests an analogous assignment for the two isomers of B_2W_8 . In particular, the isomer responsible for the ultraviolet spectrum of Fig. 6(b) and the RIDIR spectrum of Fig. 7(c) is assigned as $B_2W_8(S_4)$. The isomer with ultraviolet transitions labeled 2 in Fig. 6(a) and with the RIDIR spectrum of Fig. 7(d) is assigned as $B_2W_8(D_{2d})$. The distinction between S_4 and D_{2d}

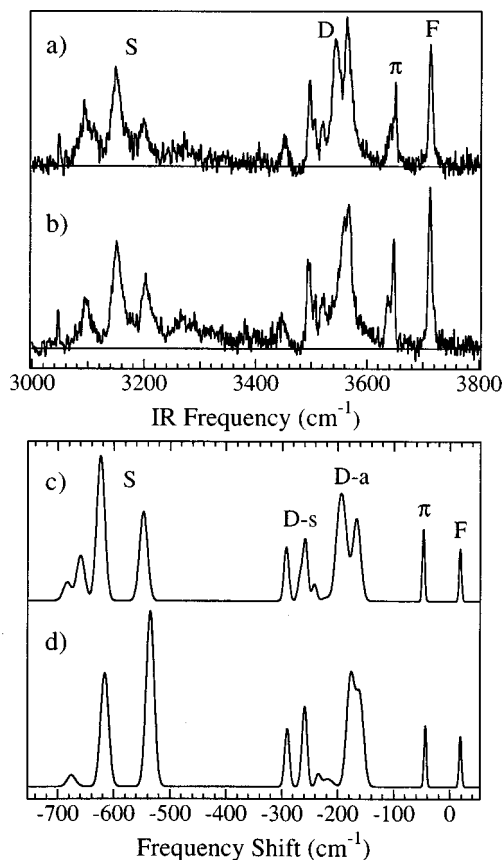


FIG. 10. Comparison of the RIDIR spectra of the BW_8 isomers [$BW_8(I)$ and $BW_8(II)$] to the calculated OH stretch spectra of the S_4 (c) and D_{2d} (d) water octamers in BW_8 . The zero of the frequency scale was taken to be the average of the symmetric and antisymmetric modes of the water monomer calculated at the same level of theory (3792 cm^{-1}). The lines in the calculated spectra were given Gaussian widths corresponding to the experimental widths of (a) and (b).

is made largely on the basis of the D - a region of the RIDIR spectrum, with Fig. 7(c) bearing the doublet signature characteristic of $W_8(S_4)$ and Fig. 7(d) the unresolved singlet of $W_8(D_{2d})$. In addition, in the R2PI spectrum of Fig. 6(a), the relative intensities and spacing of the 6_0^1 bands of $B_2W_8(S_4)$ (transitions 1) and $B_2W_8(D_{2d})$ (transitions 2) are virtually identical to those in $BW_8(S_4)$ and $BW_8(D_{2d})$.

As noted earlier, the free OH and π H-bonded OH stretch regions of the B_2W_8 isomers can be consistently assigned by assuming that the second benzene takes up a position π H-bonded to a second of the free OH groups on $W_8(S_4)$ and $W_8(D_{2d})$. This assignment accounts both for the transfer of intensity from the free OH to the π H-bonded OH region and the appearance of two π H-bonded OH stretch fundamentals. In this picture, the two benzene molecules of B_2W_8 could take up positions either on the same or opposite tetramer cycles. The present data cannot distinguish between these possibilities. From the UV-UV hole-burning spectrum of $B_2W_8(S_4)$ in Fig. 6(b), the doublet near 40 cm^{-1} (labeled 1) and the unresolved transition at 95 cm^{-1} (labeled 6) are most probably the 6_0^1 transitions of the two benzene moieties in the cluster. These transitions are approximately equally red and blue-shifted from the 6_0^1 band in $BW_8(S_4)$ (65.6 cm^{-1}). This would suggest that the two benzene mol-

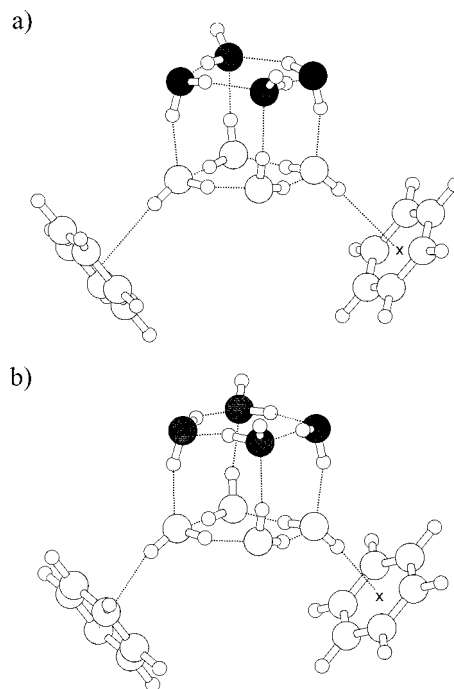


FIG. 11. Structures for the (a) $B_2W_8(S_4)$ and (b) $B_2W_8(D_{2d})$ isomers tentatively assigned as the isomers observed experimentally.

ecules do interact with one another either directly, or indirectly through the W_8 cluster. Aside from this, the B_2W_8 spectra differ from their BW_8 counterparts primarily in the look of the single-donor region.

In order to test the proposed structures for the B_2W_8 isomers, the normal modes of W_8 and BW_8 from the DFT calculations were used in a restricted normal coordinate analysis involving the set of sixteen OH bond internal coordinates. By projecting the DFT OH stretch normal modes onto the OH internal coordinates, effective OH stretch force constant matrices for W_8 and BW_8 were extracted and compared, thereby determining a force constant difference matrix ΔF .⁸⁸ A comparison of the two revealed that the major effects of benzene complexation were on the diagonal force constant matrix elements associated with the four OH groups pointing toward or away from the corner of the cube to which benzene is attached. To model the effects of the second benzene molecule, the force constant matrix for the BW_8 isomers was modified by adding to it the appropriate ΔF matrix corresponding to each of the possible points of attachment of the second benzene relative to the first. The best match with experiment is achieved for structures in which the two benzene molecules are placed on adjacent free OH groups on the same tetramer cycle [Figs. 11(a) and 11(b)]. The simulated spectra for $B_2W_8(S_4)$ and $B_2W_8(D_{2d})$ are shown in Figs. 12(a) and 12(b), respectively. The model, then, provides some evidence for the proposed structures for B_2W_8 shown in Fig. 11.

IV. DISCUSSION

The result anticipated by theory; namely, that the two lowest-energy structures for the water octamer are two nearly isoenergetic cubic structures of S_4 and D_{2d} symmetry, is

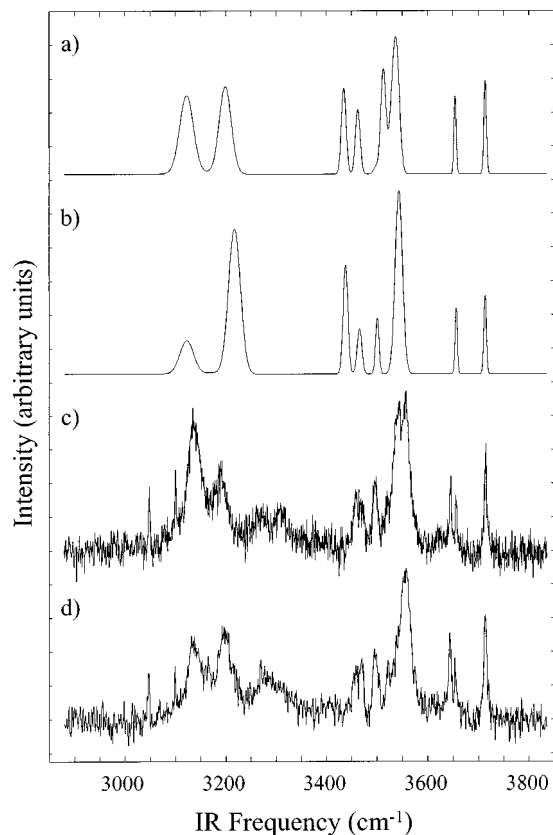


FIG. 12. Calculated OH stretch infrared spectra for the (a) $B_2W_8(S_4)$ and (b) $B_2W_8(D_{2d})$ isomers shown in Fig. 11. The simulated spectra show the expected behavior, trading intensity in the free OH for intensity in the π H-bonded OH region. The two π H-bonded OH stretch frequencies are necessarily identical in the simulation, and do not mirror the small splitting of the π fundamentals observed experimentally. The single donor region is also qualitatively reproduced, though the intensities are not quantitatively correct. See the text for further details of the calculation.

confirmed by the present experimental data on $BW_8(S_4)$, $BW_8(D_{2d})$, $B_2W_8(S_4)$, and $B_2W_8(D_{2d})$. The $W_8(S_4)$ and $W_8(D_{2d})$ isomers presented a special challenge to experiment, since they are not only the same size, but also possess near-identical H-bonding topologies (cubic) which differ primarily in the arrangement of the H-bonds. By attaching a benzene molecule to the surface of these structures and employing a combination of R2PI, UV–UV hole-burning, and RIDIR spectroscopy it has been possible to distinguish the UV spectra of the isomers and to record their OH stretch infrared spectra free from interference from one another. The 6_0^1 vibronic transitions of the two isomers are separated by only 5 cm^{-1} (out of $38\,600\text{ cm}^{-1}$), just sufficient to separate their single vibronic-level transitions for use in the double-resonance IR–UV scheme of RIDIR spectroscopy. In both BW_8 and B_2W_8 , the S_4 isomers have 6_0^1 intensities about 50% greater than their D_{2d} counterparts, suggesting a slightly greater stability for $BW_8(S_4)$ than for $BW_8(D_{2d})$.

A. The comparison with bulk and interfacial ice

The S_4 and D_{2d} cubic forms of the water octamer foreshadow some of the unique and intriguing aspects of solid ice. In particular, ice possesses more crystalline solid phases than any other known pure substance.¹ This is the case de-

spite the fact that the water molecules in all of these phases are in locally tetrahedral sites, serving as proton donor in two H-bonds and acceptor in two others. Unique structures can be formed by shuffling the hydrogens in a water lattice without significant changes in the oxygen atom positions, leading to orientational disorder in the crystal. In fact, the ice III and ice IX phases are, respectively, orientationally disordered and ordered versions of the same structure, with a phase transition between them which occurs without a measurable change in volume or x-ray diffraction pattern.¹ The S_4 and D_{2d} forms of the water octamer show that a similar versatility is present already in water clusters with as few as eight water molecules.

As noted in the introduction, the cubic S_4 and D_{2d} water octamers contain only tri-coordinate water molecules: Four with AAD (i.e., having one “dangling H”) and four with ADD bonding (i.e., having one uncoordinated oxygen lone pair). These H-bond deficient sites on the cluster are reminiscent of similar sites on the surface of bulk ice, where they are thought to be important for the binding of adsorbates to ice and the ensuing chemistry on its surface. Recently, Devlin, Buch, and co-workers^{22–26} have carried out an elegant set of studies in which they have assigned infrared spectral features of the surface and sub-surface layers of ice. These authors identify characteristic absorptions due to tri-coordinate AAD and ADD molecules, including a free OH at 3693 cm^{-1} and a single-donor OH at 3100 cm^{-1} for the AAD molecules, and absorptions at 3560 and 3330 cm^{-1} for the double-donor fundamentals of the ADD molecules. The corresponding absorptions of $BW_8(S_4)$ and $BW_8(D_{2d})$ for the $F(3713\text{ cm}^{-1})$, $S(3097/3151/3203)$, and antisymmetric double-donor (3568 cm^{-1}) are striking, though the symmetric double-donor transitions ($3446\text{--}3523$) are not as good a match. Of course, in BW_8 , the single-donor transitions are shifted and split by the presence of benzene. However, the comparison of the single-donor transitions in free W_8 from the work of Buch and Buck ($\sim 3100\text{ cm}^{-1}$) is encouraging.⁴⁴ Thus, it appears that water clusters as small as the water octamer possess infrared absorptions similar to those of tri-coordinate water molecules at the surface of ice. This raises the prospect of using water clusters as models for processes occurring at ice surfaces.

One must not surmise on this basis that all double-donor water molecules will absorb in the region near 3550 cm^{-1} . On the contrary, in ice Ih, all water molecules are tetra coordinated and double donor, but only a single maximum near 3200 cm^{-1} is present. In this case, the locally tetrahedral geometry allows strong, nearly linear H-bonds with large frequency shifts from the free OH region. By contrast, in $W_8(S_4)$ and $W_8(D_{2d})$, the double-donor water molecules are constrained to the corners of a cube, producing nonlinear H-bonds with calculated O–O separations 0.17 \AA longer than their single-donor counterparts. The result is the signature cubic or cuboid double-donor OH absorptions near 3550 cm^{-1} . Given the similar absorption frequencies of tri-coordinate ADD molecules on the surface of ice, a similar strain and O–O separation must be present there.

B. π H-bonding in BW_8 and B_2W_8

There are several features of the experimental and calculated results which shed light on the π H-bond between cubic W_8 and benzene. First, the frequency of the π H-bonded OH stretch ($3650/3648\text{ cm}^{-1}$ in S_4/D_{2d} BW_8) is very similar to that found in BW_4 (3651 cm^{-1}) and BW_5 (3647 cm^{-1}).⁴ That this is so may reflect the fact that $W_8(S_4)$ and $W_8(D_{2d})$, like the cyclic W_3 – W_5 species, are nonpolar. The insensitivity of the π H-bond to the size of the cycle (in W_{3-5}) or the presence of a second layer (in W_8), suggests that the π H-bond is a local interaction primarily with a single water molecule in the cluster. Recently, Devlin and co-workers⁸⁹ have obtained difference infrared spectra of ice nanocrystals with and without benzene physisorbed to the surface. With benzene present, the free OH stretch for AAD water molecules shifts from 3696 to 3575 cm^{-1} under the influence of the π H-bond with benzene. This shift (-121 cm^{-1}) is about twice that found in $BW_8(S_4)$ (-56 cm^{-1}) and $BW_8(D_{2d})$ (-58 cm^{-1}). To date, the largest shift due to π H-bond formation between benzene and a water cluster is found in the BW_7 cluster (-72 cm^{-1}),⁴ still well short of that in interfacial ice.

The 7 cm^{-1} intermolecular vibrational frequency observed in the R2PI spectra of both isomers is consistent with the notion of a floppy intermolecular coordinate, probably involving $B\cdots W_8$ libration. Furthermore, the π H-bonded OH stretch fundamental from the RIDIR spectroscopy consists of two partially resolved transitions separated by about 10 cm^{-1} . One plausible explanation for this doublet would be to ascribe it to large-amplitude motions (LAMs) of the π bound OH as W_8 undergoes its zero-point motion. In the 1:1 benzene– H_2O complex, the OH stretch infrared spectrum showed extensive combination-band structure due to the LAMs present in the complex.⁵⁸ A similar mechanism for inducing intensity in a low-frequency librational combination band may be operating in the BW_8 clusters.

C. The dynamics of H-bonded networks

The dynamics of the H-bonded network is also reflected in the mode-selective breadths of the individual bands, which are included in Table II. Given the bandwidth of our OPO ($\sim 1.5\text{ cm}^{-1}$), the inherent breadths observed for the free OH stretch and π H-bonded OH stretch transitions are not determined. Nevertheless, these bands are clearly several times narrower than the double-donor and single-donor vibrations, whose approximate widths are given in Table II. Given the close correspondence between the experimental and calculated OH stretch spectra, these widths (especially in the single-donor region) cannot be ascribed to unresolved OH stretch bands, since essentially all bands are accounted for. Instead, one must conclude that the single-donor and double-donor modes that are intimately involved in the H-bonded network are more strongly coupled to the background states than are the modes associated with the OH groups that are peripheral to the cube. If coherently prepared, the vibrational relaxation into this bath would occur on a time scale of about 300 fs.

D. Coating, trapping, and expanding the cube

Several avenues for future study are raised by the present work. First, given the structures deduced for BW_8 and B_2W_8 , one wonders whether it might be possible to cap all four free OH groups with benzene, thereby coating its surface with benzene. Such a B_4W_8 structure would be anticipated on symmetry grounds to have a spectrum very close to that of free W_8 , but with all free OH transitions removed in favor of additional π H-bonding intensity. The beauty of this structure would alone be sufficient justification for pursuing its study.

Second, the recent x-ray crystallographic identification⁹⁰ of a cubic W_8 cluster of C_i symmetry trapped in a molecular cavity opens the possibility of devising similar cavities with H-bonding groups positioned so as to trap other of the four-teen W_8 cubic structures, including $W_8(S_4)$ and $W_8(D_{2d})$.

Finally, given the unique stability of the cubic structures, it is not surprising that these structures can be expanded to accommodate additional water molecule(s) in similarly stable structures. We will report elsewhere on two isomers of BW_9 which have spectra consistent with precisely such structures.⁸⁶ The recent, elegant work of Buck and co-workers⁴⁴ on the free W_9 and W_{10} clusters are also interpreted as arising from similar structures. Whether even larger clusters will favor fused cubic structures over other H-bonded networks is a completely open question deserving future study.

ACKNOWLEDGMENTS

We gratefully acknowledge NSF for support of this research under grant Nos. CHE-9728636 and CHE-9422210. C. J. G. thanks Lubrizol Corp. for a graduate fellowship. Some of the calculations were carried out on the HP Exemplar computer at NCSA. The authors further thank C. Sosa of SGI Cray and V. Balaji of NCSA for assistance with some of the calculations. The authors also thank J. P. Devlin, V. Buch, and U. Buck for sharing their results prior to publication.

¹E. Whalley, in *The Hydrogen Bond, Vol. III*, edited by P. Schuster, G. Zundel, and C. Sandorfy (North-Holland, Amsterdam, 1976), pp. 1427–1470.

²A. K. Soper and M. G. Phillips, *Chem. Phys.* **107**, 47 (1986).

³K. Liu, J. D. Cruzan, and R. J. Saykally, *Science* **271**, 929 (1995).

⁴R. N. Pribble and T. S. Zwier, *Science* **265**, 75 (1994).

⁵K. Liu, J. K. Gregory, M. G. Brown, C. Carter, R. J. Saykally, and D. C. Clary, *Nature (London)* **381**, 501 (1996).

⁶F. H. Stillinger and C. W. David, *J. Chem. Phys.* **73**, 3384 (1980).

⁷D. A. Estrin, L. Paglieri, G. Corongui, and E. Clementi, *J. Phys. Chem.* **100**, 8701 (1996).

⁸C. Lee, H. Chen, and G. Fitzgerald, *J. Chem. Phys.* **102**, 1266 (1995).

⁹J. O. Jensen, P. N. Krishnan, and L. A. Burke, *Chem. Phys. Lett.* **246**, 13 (1995).

¹⁰K. S. Kim, B. J. Mhin, S. J. Lee, and K. S. Kim, *Chem. Phys. Lett.* **219**, 243 (1994).

¹¹R. Knochenmuss and S. Leutwyler, *J. Chem. Phys.* **96**, 5233 (1992).

¹²C. J. Gruenloh, J. R. Carney, C. A. Arrington, T. S. Zwier, S. Y. Fredericks, and K. D. Jordan, *Science* **276**, 1678 (1997).

¹³C. J. Tsai and K. D. Jordan, *J. Phys. Chem.* **97**, 5208 (1993).

¹⁴G. Brink and L. Glasser, *J. Phys. Chem.* **88**, 3412 (1984).

¹⁵K. S. Kim, M. Dupuis, G. C. Lie, and E. Clementi, *Chem. Phys. Lett.* **131**, 451 (1986).

¹⁶C. J. Tsai and K. D. Jordan, *J. Chem. Phys.* **95**, 3850 (1991).

- ¹⁷D. J. Wales and I. Ohmine, *J. Chem. Phys.* **98**, 7257 (1993).
- ¹⁸R. J. Wawak, M. M. Wimmer, and H. A. Scherega, *J. Phys. Chem.* **96**, 5138 (1992).
- ¹⁹S. C. Farantos, S. Kapetanakis, and A. Vegiri, *J. Phys. Chem.* **97**, 12158 (1993).
- ²⁰S. McDonald, S. J. Singer, and L. Ojamae, *J. Phys. Chem.* **102**, 2824 (1998).
- ²¹C. J. Tsai and K. D. Jordan (unpublished results).
- ²²J. P. Devlin, *Int. Rev. Phys. Chem.* **9**, 29 (1990).
- ²³B. Rowland, N. S. Kadagathur, J. P. Devlin, V. Buch, T. Feldman, and M. J. Wojcik, *J. Chem. Phys.* **102**, 8328 (1995).
- ²⁴V. Buch, L. Delzeit, C. Blackledge, and J. P. Devlin, *J. Phys. Chem.* **100**, 3732 (1996).
- ²⁵L. Delzeit, M. S. Devlin, B. Rowland, and J. P. Devlin, *J. Phys. Chem.* **100**, 10076 (1996).
- ²⁶L. Delzeit, J. P. Devlin, and V. Buch, *J. Chem. Phys.* **107**, 3726 (1997).
- ²⁷Q. Du, R. Superfine, E. Freysz, and Y. R. Shen, *Phys. Rev. Lett.* **70**, 2313 (1993).
- ²⁸D. J. Wales, *J. Am. Chem. Soc.* **115**, 11180 (1993).
- ²⁹L. S. Sremaniak, L. Perera, and M. L. Berkowitz, *J. Chem. Phys.* **105**, 3715 (1996).
- ³⁰L. Ojamae, J. Tegenfeldt, J. Lindgren, and K. Hermansson, *Chem. Phys. Lett.* **195**, 97 (1992).
- ³¹C. E. Dykstra, *J. Chem. Phys.* **91**, 6472 (1989).
- ³²J. D. Augspurger, C. E. Dykstra, and T. S. Zwier, *J. Phys. Chem.* **97**, 980 (1993).
- ³³C. Millot and A. J. Stone, *Mol. Phys.* **77**, 439 (1992).
- ³⁴M. F. Vernon, D. J. Drajnovich, H. S. Kwok, J. M. Lisy, Y. R. Shen, and Y. T. Lee, *J. Chem. Phys.* **77**, 47 (1982).
- ³⁵R. H. Page, J. G. Frey, Y. R. Shen, and Y. T. Lee, *Chem. Phys. Lett.* **106**, 373 (1984).
- ³⁶D. F. Coker, R. E. Miller, and R. O. Watts, *J. Chem. Phys.* **82**, 3554 (1985).
- ³⁷S. Wuelfert, D. Herren, and S. Leutwyler, *J. Chem. Phys.* **86**, 3751 (1987).
- ³⁸F. Huisken, M. Kaloudis, and A. Kulcke, *J. Chem. Phys.* **104**, 17 (1996).
- ³⁹F. Huisken, in *Molecular Complexes in the Earth's, Planetary, and Cometary Atmospheres*, edited by Z. S. J.-F. Crifo and A. A. Vigasin (World Scientific, Singapore, 1997).
- ⁴⁰J. D. Cruzan, L. B. Braly, K. Liu, M. G. Brown, J. G. Loeser, and R. J. Saykally, *Science* **271**, 59 (1996).
- ⁴¹K. Liu, M. G. Brown, J. D. Cruzan, and R. J. Saykally, *Science* **271**, 62 (1996).
- ⁴²R. Frochtenicht, M. Kaloudis, M. Koch, and F. Huisken, *J. Chem. Phys.* **105**, 6128 (1996).
- ⁴³K. Liu, M. G. Brown, and R. J. Saykally, *J. Phys. Chem. A* **101**, 8995 (1997).
- ⁴⁴U. Buck, I. Ettischer, M. Melzer, V. Buch, and J. Sadlej, *Phys. Rev. Lett.* **80**, 2578 (1998).
- ⁴⁵U. Buck and H. Meyer, *Phys. Rev. Lett.* **52**, 109 (1984).
- ⁴⁶U. Buck, X. Gu, C. Lauenstein, and A. Rudolph, *J. Phys. Chem.* **92**, 5561 (1988).
- ⁴⁷R. N. Pribble and T. S. Zwier, *Faraday Discuss.* **97**, 229 (1994).
- ⁴⁸R. H. Page, Y. R. Shen, and Y. T. Lee, *J. Chem. Phys.* **88**, 5362 (1988).
- ⁴⁹G. V. Hartland, B. F. Henson, V. A. Venturo, and P. M. Felker, *J. Phys. Chem.* **96**, 1164 (1992).
- ⁵⁰P. M. Felker, *Chem. Rev.* **94**, 1784 (1994).
- ⁵¹T. Ebata, N. Mizuochi, T. Watanabe, and N. Mikami, *J. Phys. Chem.* **100**, 546 (1996).
- ⁵²A. Fujii, S. Okuyama, T. Maeyama, T. Ebata, and N. Mikami, *Chem. Phys. Lett.* **256**, 1 (1996).
- ⁵³A. Iwasaki, A. Fujii, T. Watanabe, T. Ebata, and N. Mikami, *J. Phys. Chem.* **100**, 16053 (1996).
- ⁵⁴T. Watanabe, T. Ebata, S. Tanabe, and N. Mikami, *J. Chem. Phys.* **105**, 408 (1996).
- ⁵⁵C. Riehn, C. Lahmann, B. Wassermann, and B. Brutschy, *Ber. Bunsenges. Phys. Chem.* **96**, 1161 (1992).
- ⁵⁶C. Riehn, C. Lahmann, B. Wassermann, and B. Brutschy, *Chem. Phys. Lett.* **197**, 443 (1992).
- ⁵⁷S. Djafari, G. Lembach, H. D. Barth, and B. Brutschy, *Z. Phys. Chem. (Munich)* **195**, 253 (1996).
- ⁵⁸R. N. Pribble, A. W. Garrett, K. Haber, and T. S. Zwier, *J. Chem. Phys.* **103**, 531 (1995).
- ⁵⁹R. N. Pribble, C. Gruenloh, and T. S. Zwier, *Chem. Phys. Lett.* **262**, 627 (1996).
- ⁶⁰R. N. Pribble, F. Hagemester, and T. S. Zwier, *J. Chem. Phys.* **106**, 2145 (1997).
- ⁶¹C. J. Gruenloh and T. S. Zwier, *Size- and Conformation-selective infrared spectroscopy of neutral hydrogen-bonded clusters* (submitted).
- ⁶²A. J. Gotch and T. S. Zwier, *J. Chem. Phys.* **96**, 3388 (1992).
- ⁶³A. W. Garrett and T. S. Zwier, *J. Chem. Phys.* **96**, 3402 (1992).
- ⁶⁴E. Wahlraefen, *J. Chem. Phys.* **47**, 114 (1967).
- ⁶⁵C. Lee, W. Yang, and R. G. Parr, *Phys. Rev. B* **37**, 785 (1988).
- ⁶⁶A. D. Becke, *J. Chem. Phys.* **98**, 5648 (1993).
- ⁶⁷M. J. Frisch, J. A. Pople, and J. S. Binkley, *J. Chem. Phys.* **80**, 3265 (1984).
- ⁶⁸C. Lee, H. Chen, and G. Fitzgerald, *J. Chem. Phys.* **101**, 4472 (1994).
- ⁶⁹K. Kim and K. D. Jordan, *J. Phys. Chem.* **98**, 11089 (1992).
- ⁷⁰S. S. Xantheas, *J. Chem. Phys.* **102**, 4505 (1995).
- ⁷¹L. Gonzalez, O. Mo, M. Yanez, and J. Elguero, *J. Mol. Struct.: THEOCHEM* **371**, 1 (1996).
- ⁷²F. C. Hagemester, C. J. Gruenloh, and T. S. Zwier, *J. Phys. Chem. A* **102**, 82 (1998).
- ⁷³S. Fredericks, K. D. Jordan, and T. S. Zwier, *J. Phys. Chem.* **100**, 7810 (1996).
- ⁷⁴W. J. Hehre, R. Ditchfield, and J. A. Pople, *J. Chem. Phys.* **56**, 2257 (1972).
- ⁷⁵T. Clark, J. Chandrasekhar, G. W. Spitznagel, and P. v. R. Schleyer, *J. Comput. Chem.* **4**, 294 (1983).
- ⁷⁶P. Nachtigall, K. D. Jordan, A. Smith, and H. Jonsson, *J. Chem. Phys.* **104**, 148 (1996).
- ⁷⁷K. D. Jordan (unpublished).
- ⁷⁸M. J. Frisch, G. W. Trucks, H. B. Schlegel, P. M. W. Gill, B. G. Johnson, M. A. Robb, J. R. Cheeseman, T. A. Keith, G. A. Petersson, J. A. Montgomery, K. Raghavachari, M. A. Al-Laham, V. G. Zakrzewski, J. V. Ortiz, J. B. Foresman, C. Y. Peng, P. Y. Ayala, W. Chen, M. W. Wong, J. L. Andres, E. S. Replogle, R. Gomperts, R. L. Martin, D. J. Fox, J. S. Binkley, D. J. Defrees, J. Baker, J. P. Stewart, M. Head-Gordon, C. Gonzalez, and J. A. Pople, *GAUSSIAN 94*, Revision B.3, Gaussian, Inc., Pittsburgh PA, 1995.
- ⁷⁹S. F. Boys and F. Bernardi, *Mol. Phys.* **19**, 553 (1970).
- ⁸⁰A. W. Garrett, D. L. Severance, and T. S. Zwier, *J. Chem. Phys.* **96**, 7245 (1992).
- ⁸¹A. W. Garrett, and T. S. Zwier, *J. Phys. Chem.* **96**, 9710 (1992).
- ⁸²J. R. Carney, F. C. Hagemester, and T. S. Zwier, *J. Chem. Phys.* **108**, 3379 (1998).
- ⁸³A. J. Gotch, A. W. Garrett, D. L. Severance, and T. S. Zwier, *Chem. Phys. Lett.* **178**, 121 (1991).
- ⁸⁴K. Kim, K. D. Jordan, and T. S. Zwier, *J. Am. Chem. Soc.* **116**, 11568 (1994).
- ⁸⁵A. J. Gotch and T. S. Zwier, *J. Chem. Phys.* **93**, 6977 (1990).
- ⁸⁶C. J. Gruenloh, F. C. Hagemester, J. R. Carney, T. S. Zwier, J. T. Wood III, S. Y. Fredericks, and K. D. Jordan (manuscript in preparation).
- ⁸⁷See AIP Document No. E-PAPS: E-JCPSA6-109-001840 for further details of the DFT Becke3LYP calculations on W_8 and BW_8 including (i) their structures, (ii) binding energies, (iii) dipole moments, (iv) isomeric forms, and (v) OH stretch normal modes. E-PAPS document files may be retrieved free of charge from our FTP server (<http://www.aip.org/epaps/epaps.html>) or from [ftp.aip.org](ftp://ftp.aip.org) in the directory /epaps/. For further information, e-mail: paps@aip.org or fax: 516-576-2223.
- ⁸⁸E. Honegger and S. Leutwyler, *J. Chem. Phys.* **88**, 2582 (1988).
- ⁸⁹S. C. Silva and J. P. Devlin, *J. Phys. Chem.* **98**, 10847 (1994).
- ⁹⁰W. B. Blanton, S. W. Gordon-Wylie, K. D. Jordan, J. T. Wood, G. Clark, and T. J. Collins, *Nature* (submitted).